

Electronic Supplementary Information

Supramolecular activation of a molecular photocatalyst

Michael G. Pfeffer, Christian Pehlken, Robert Staehle, Dieter Sorsche, Carsten Streb and
Sven Rau

If not mentioned otherwise all experiments were performed under aerobic conditions.

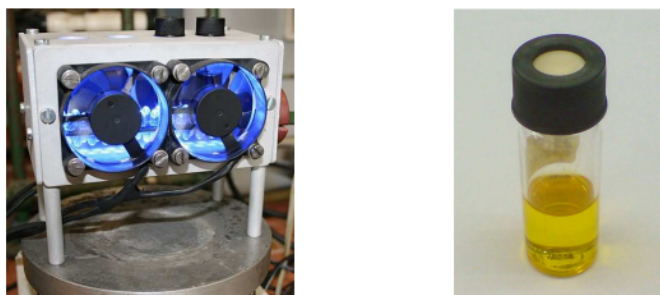


Figure S1 Photomicroreactor with air ventilation and LED irradiation (left) and a commercial available GC vial with septum containing the catalytic mixture (right).

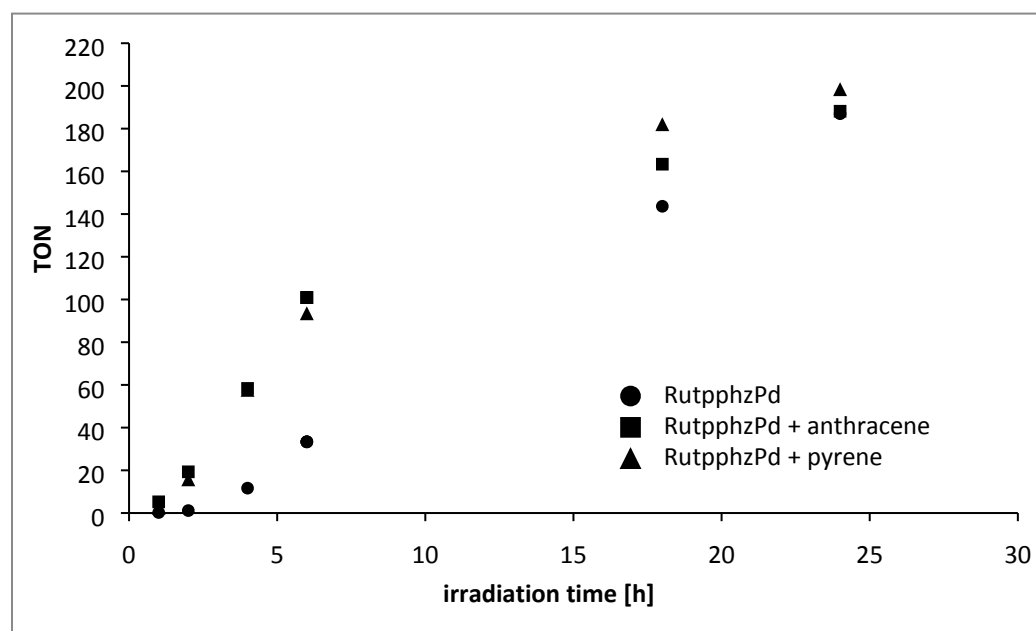


Figure S2 Long-term irradiation: catalytic hydrogen production of **RutpphzPd** ($c = 70 \mu\text{M}$), **RutpphzPd** + anthracene (80-fold excess) and **RutpphzPd** + pyrene (80-fold excess) depending on the irradiation time; $\text{TON} = n(\text{H}_2)/n(\text{RutpphzPd})$.

t [h]	1	2	4	6	18	24
TON (std. dev.) RutpphzPd	0.3 (0.2)	1.2 (0.1)	11.7 (0.8)	33.7 (4.5)	143.7 (12.1)	187.0 (9.9)
TON (std. dev.) RutpphzPd + anthracene	5.3 (0.5)	19.3 (2.0)	58.4 (2.8)	100.9 (0.6)	163.4 (2.5)	188.2 (17.0)
TON (std. dev.) RutpphzPd + pyrene	2.2 (0.6)	15.5 (0.6)	57.4 (9.2)	93.3 (5.0)	181.8 (0.3)	198.2 (9.2)

Table S1 Turnover numbers and standard deviation (in brackets) of the photocatalytic hydrogen production of **RutpphzPd** ($c = 70 \mu\text{M}$), **RutpphzPd** + anthracene (80-fold excess) and **RutpphzPd** + pyrene (80-fold excess) depending on the irradiation time; TON = $n(\text{H}_2)/n(\text{RutpphzPd})$.

¹H-NMR Spectroscopy

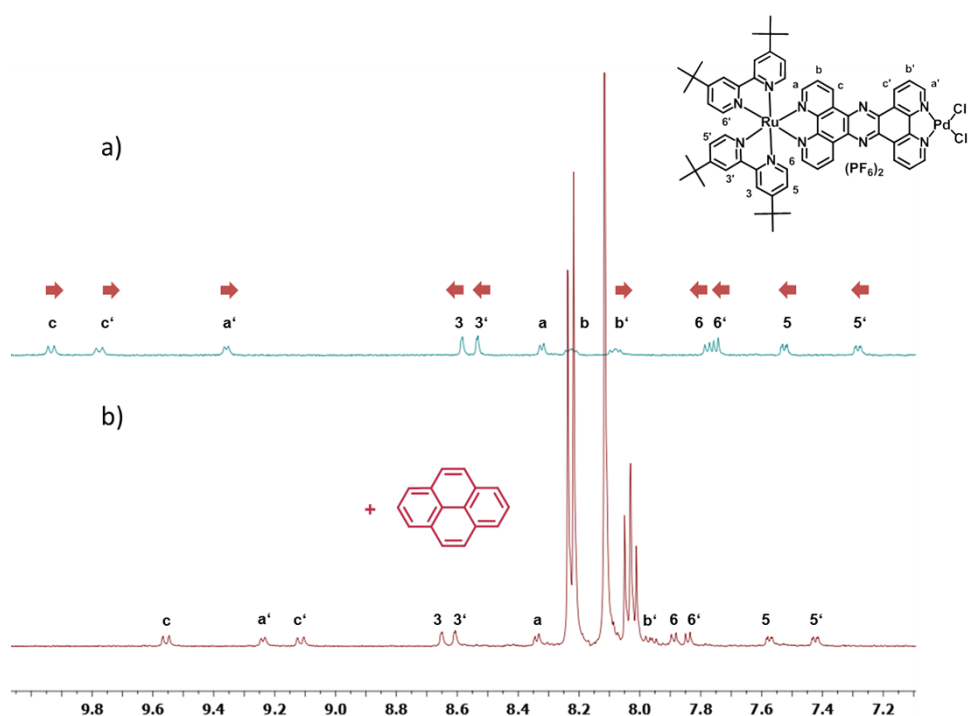


Figure S3 Changes in the ¹H-NMR spectrum of **RutpphzPd** with the addition of pyrene: (a) ¹H-NMR spectrum of **RutpphzPd** ($c = 1\text{ mM}$) in acetonitrile- d_3 ; (b) ¹H-NMR spectrum after the addition of pyrene ($c = 10\text{ mM}$).

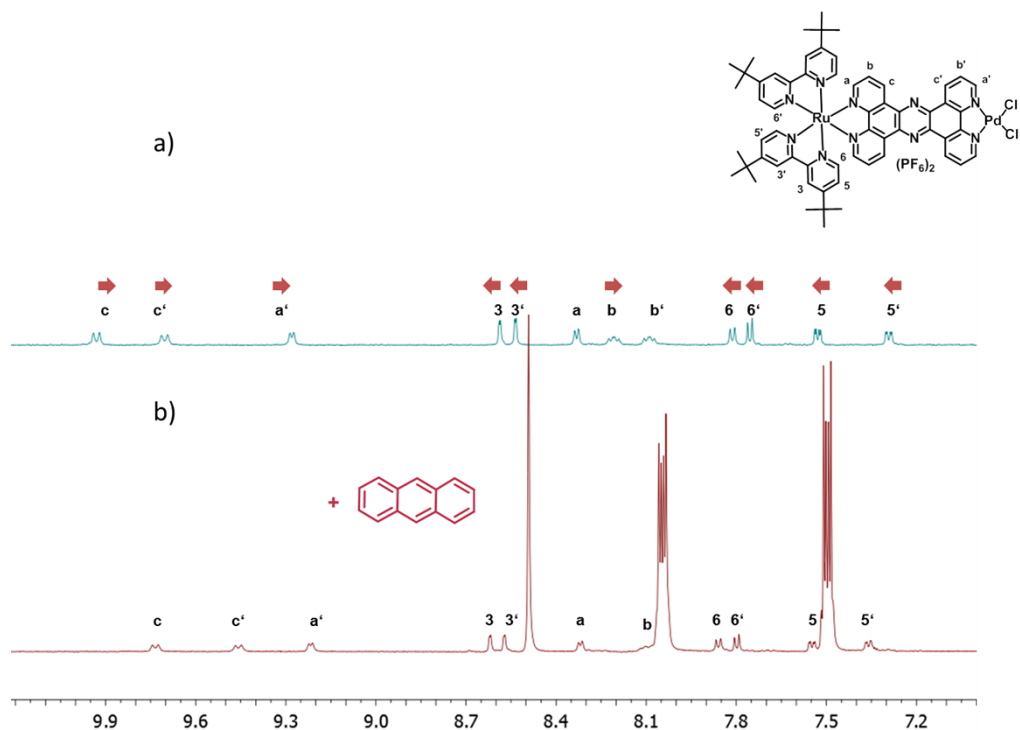


Figure S4 Changes in the ¹H-NMR spectrum of **RutpphzPd** with the addition of anthracene: a) ¹H-NMR spectrum of **RutpphzPd** ($c = 1\text{ mM}$) in acetonitrile- d_3 ; b) ¹H-NMR spectrum after the addition of anthracene ($c = 10\text{ mM}$).

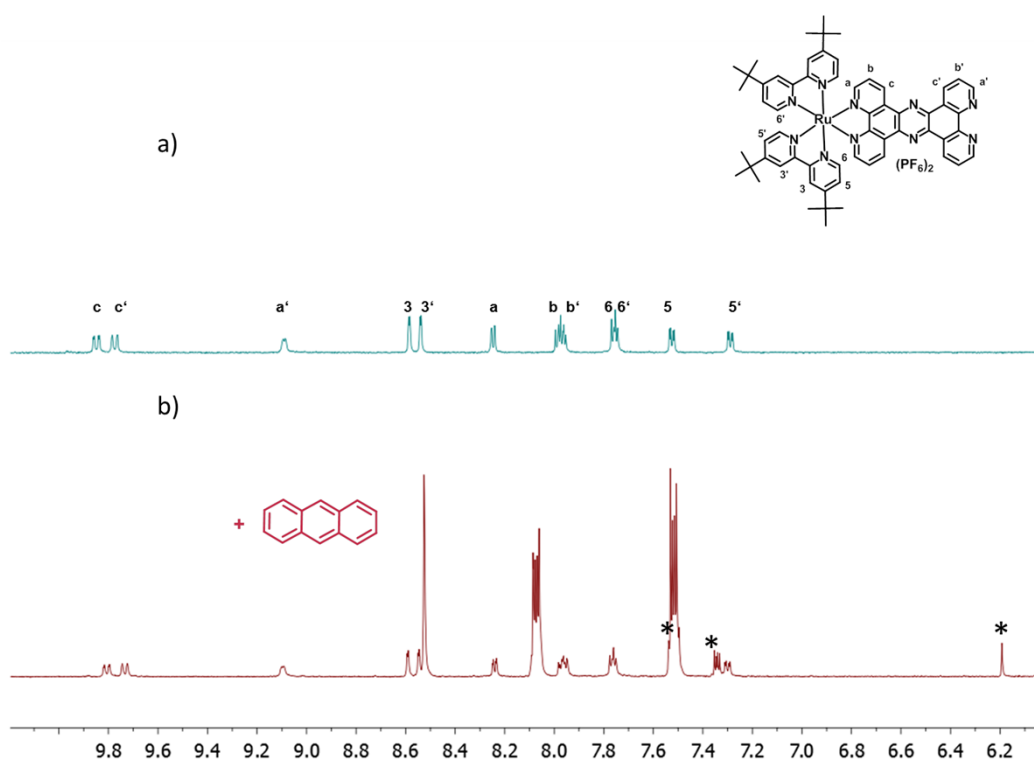


Figure S5 Changes in the ^1H -NMR spectrum of **Rutpphz** with the addition of anthracene : (a) ^1H -NMR spectrum of **Rutpphz** ($c = 1 \text{ mM}$) in acetonitrile- d_3 ; (b) ^1H -NMR spectrum after the addition of anthracene ($c = 10 \text{ mM}$) and short exposure to ambient light; *signals of anthracene dimer

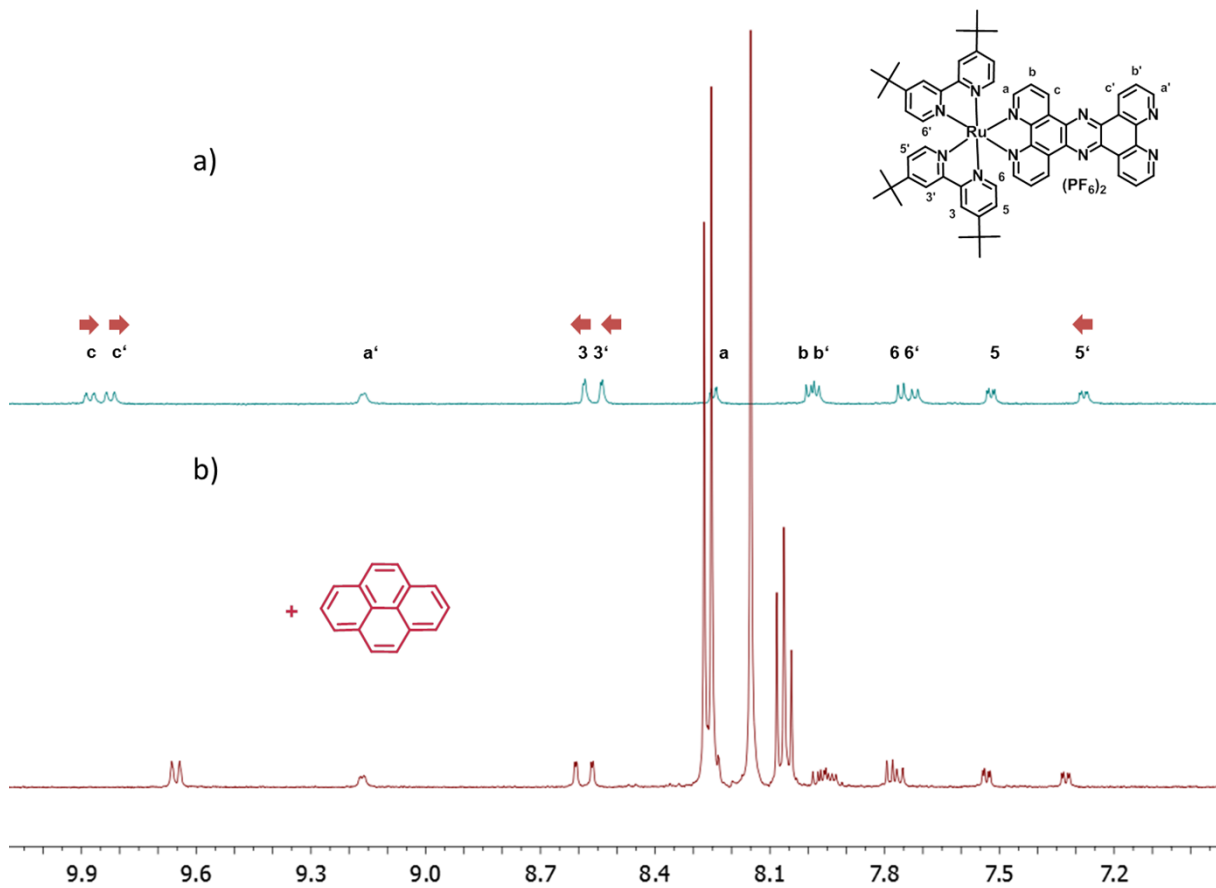


Figure S6 Changes in the ¹H-NMR spectrum of **Rutpphz** with the addition of pyrene : (a) ¹H-NMR spectrum of **Rutpphz** ($c = 1 \text{ mM}$) in acetonitrile- d_3 ; (b) ¹H-NMR spectrum after the addition of pyrene ($c = 10 \text{ mM}$).

Determination of association of **RutpphzPd** and pyrene constant via concentration dependent ¹H-NMR spectroscopy

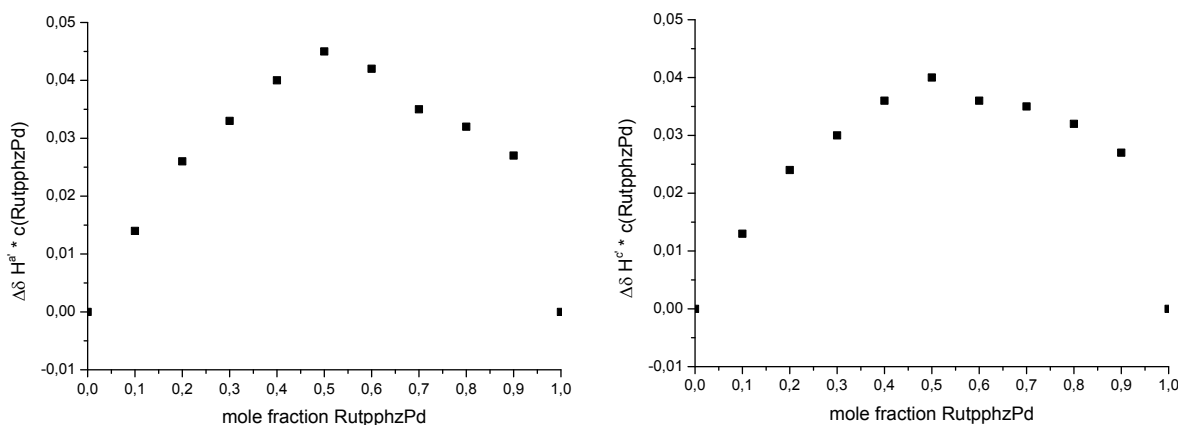


Figure S7 Analysis of **RutpphzPd**-pyrene binding stoichiometry by Job plot^[1]. Therefore $\Delta\delta^{*} c(\text{RutpphzPd})$ of the protons $H^{a'}$ and H^c is plotted against the mole fraction of **RutpphzPd**. Both graphs show a maximum at 0.5 depicting a 1/1 stoichiometry for the **RutpphzPd**-pyrene adduct. $0.2 \times 10^{-4} \text{ M} \leq [\text{RutpphzPd}] \leq 2.0 \times 10^{-4} \text{ M}$.

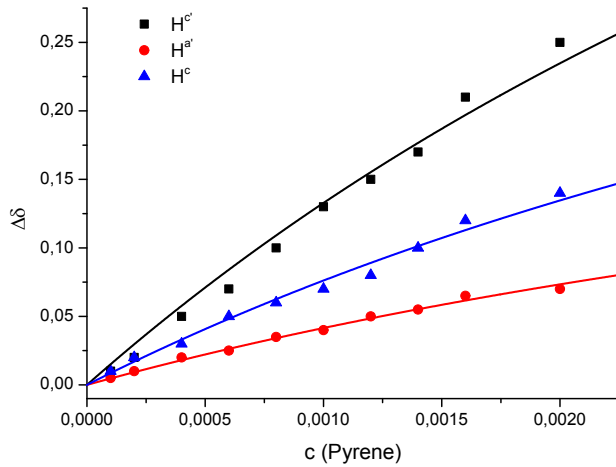
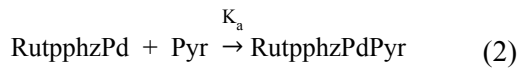


Figure S8 Non linear global curve fitting of concentration dependent ^1H -NMR spectroscopy of **RutpphzPd** and pyrene. Therefore $\Delta\delta = \delta_0 - \delta$ of the protons c' , a' and c is plotted against the concentration of pyrene, where δ is the chemical shift of the **RutpphzPd**-pyrene adduct and δ_0 is the chemical shift of pure **RutpphzPd**. The fit was performed with eq. (1)^{[1],[2]} and gives the association constant $K_a = 155 \pm 44 \text{ M}^{-1}$ for the interaction between pyrene and the π -system of the tpphz ligand. $[\text{RutpphzPd}]_0 = 1 * 10^{-4} \text{ M}$.

Fit statistics: reduced $\chi^2 = 4.64 * 10^{-5}$, adjusted $R^2 = 0.988$.

$$\Delta\delta = \delta_{\Delta\text{RutpphzPdPyr}} = \frac{(K_a[\text{RutpphzPd}]_0 + K_a[\text{Pyr}]_0 + 1) - \sqrt{(K_a[\text{RutpphzPd}]_0 - K_a[\text{Pyr}]_0)^2 + 2K_a[\text{RutpphzPd}]_0}}{2K_a[\text{RutpphzPd}]_0} \quad (1)$$

Determination of the potential equilibrium constant in the catalytic mixture



$$K_a = \frac{[\text{RutpphzPdPyr}]}{[\text{RutpphzPd}] * [\text{Pyr}]} \quad (3)$$

$$[\text{RutpphzPd}] = [\text{RutpphzPd}]_0 - [\text{RutpphzPdPyr}] \quad (4)$$

$$[\text{Pyr}] = [\text{Pyr}]_0 - [\text{RutpphzPdPyr}] \quad (5)$$

$$[\text{RutpphzPdPyr}] = \frac{(K_a[\text{RutpphzPd}]_0 + K_a[\text{Pyr}]_0 + 1) - \sqrt{(K_a[\text{RutpphzPd}]_0 + K_a[\text{Pyr}]_0 + 1)^2 - 4 * K_a^2[\text{RutpphzPd}]_0[\text{Pyr}]}}{2K_a} \quad (6)$$

¹H-NMR Concentration dependency of Rutpphz and RutpphzPd

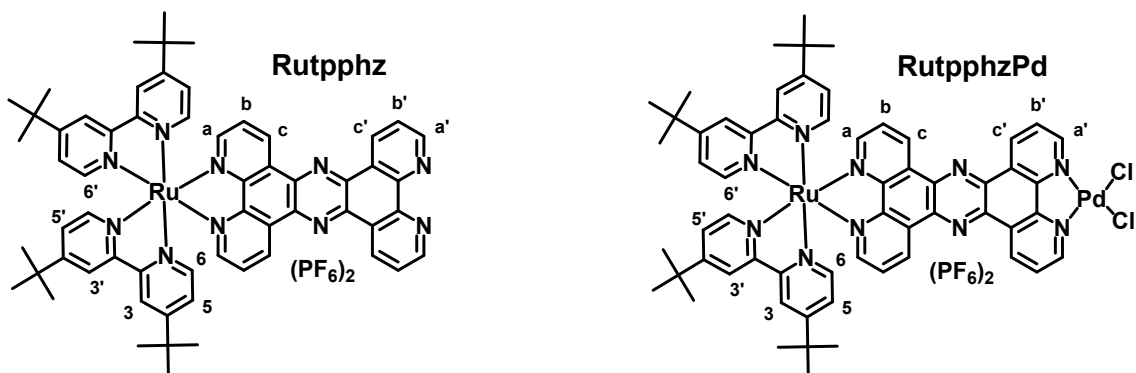


Figure S9 ¹H-NMR signal assignment of **Rutpphz** and **RutpphzPd**.

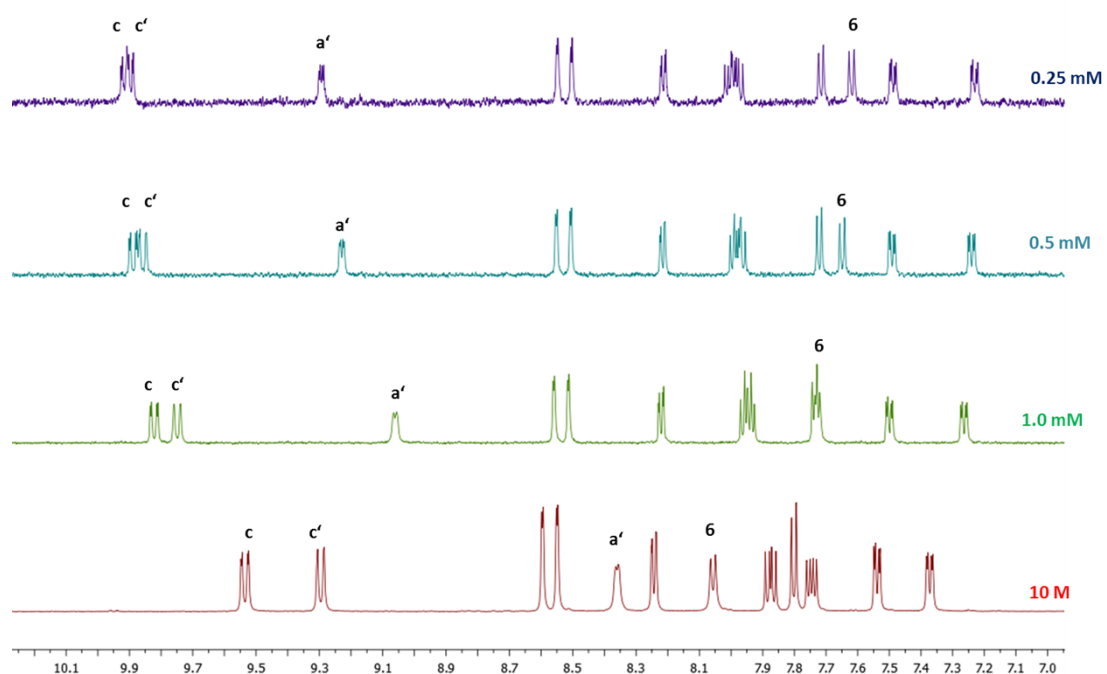


Figure S10 ¹H-NMR spectra of **Rutpphz** in acetonitrile-d₃ at different concentrations (0.25 mM to 10 mM).

Dimerization constant of Rutpphz

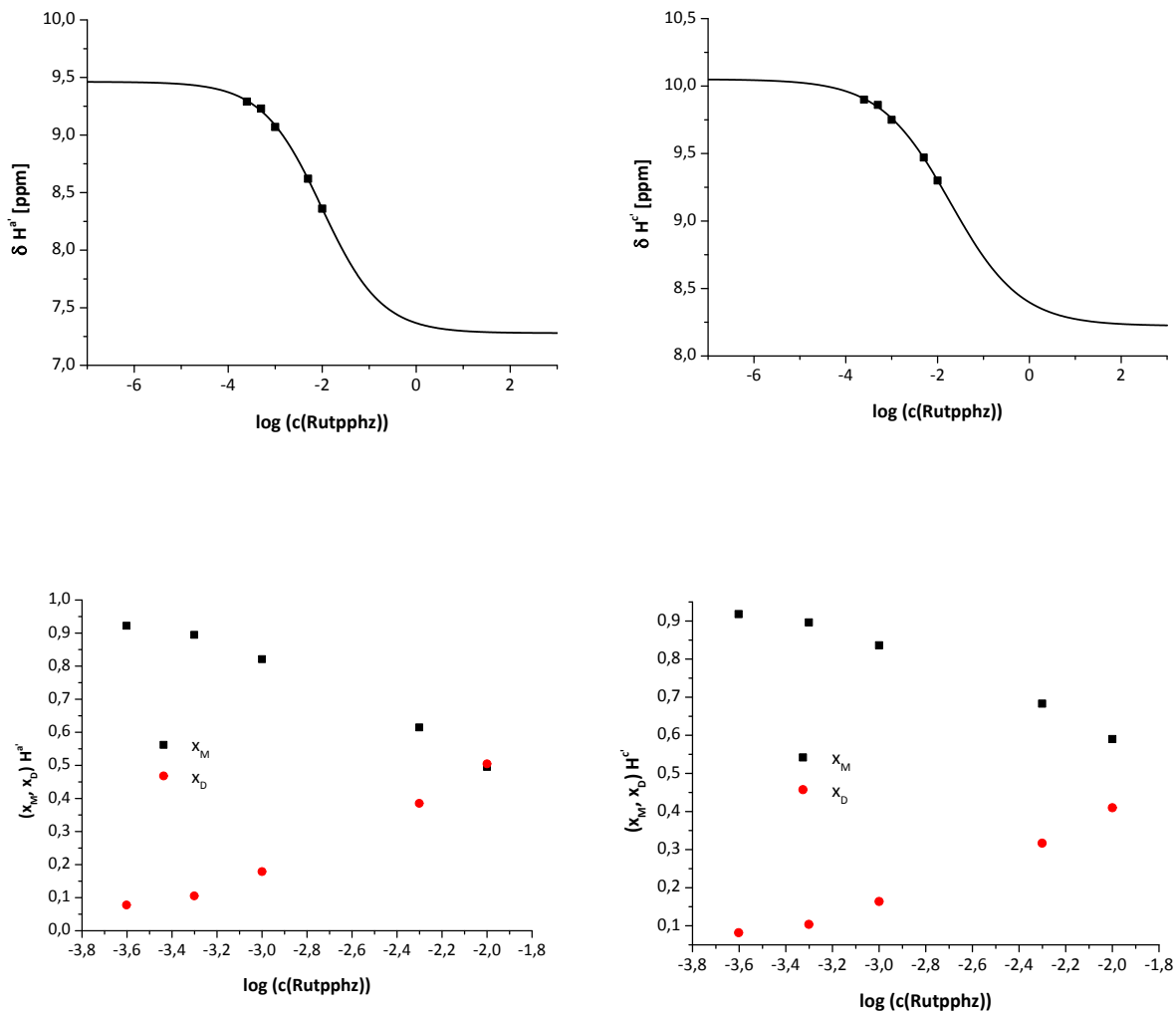


Figure S11 Analysis of the ^1H -NMR data of proton a' and c' of **Rutpphz** at different concentrations for the determination of $K_D^{[3]}$; top: change of the chemical shift of H^a' and H^c' as a function of $c(\text{Rutpphz})$. Bottom: calculated mole fraction x_M and x_D for the monomer and the dimer.

$K_D H^c'$	$K_D H^a'$
$113 \pm 10 \text{ M}^{-1}$	$131 \pm 10 \text{ M}^{-1}$
$K_D(\text{av}) = 122 \pm 19 \text{ M}^{-1}$	

Table S2 K_D values for protons H^c' and H^a' and the average K_D value.

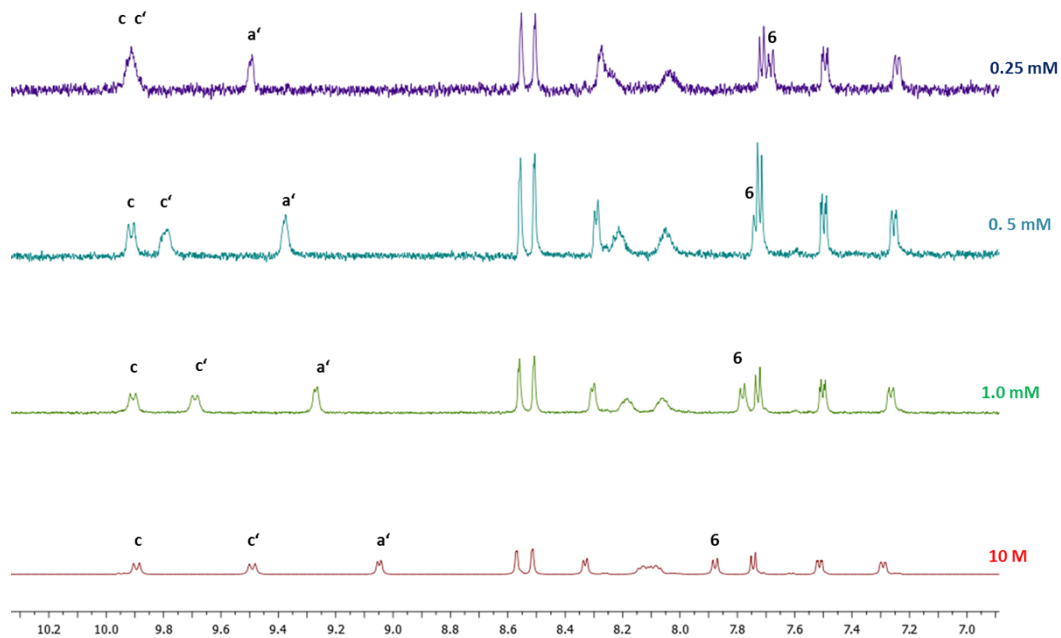


Figure S12 ^1H -NMR spectra of **RutpphzPd** in acetonitrile- d_3 at different concentrations (0.25 mM to 10 mM).

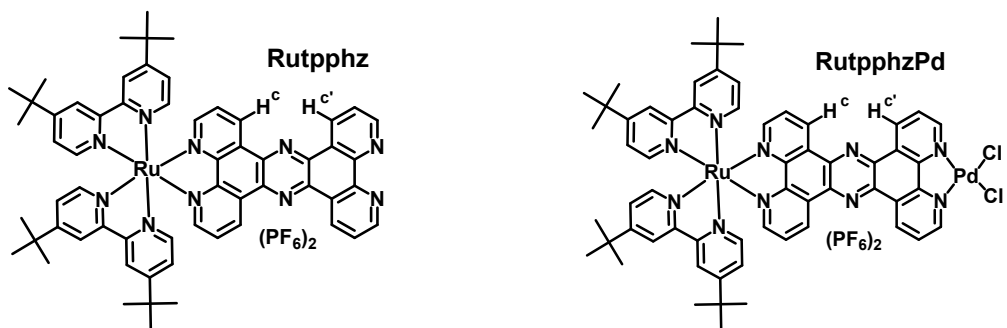


Table S3 ^1H -NMR concentration dependency of **Rutpphz** (left) and **RutpphzPd** (right) in acetonitrile- d_3 with regard to the chemical shifts of protons $\text{H}^c, \text{H}^{c'}, \text{H}^{a'}$ and H^6 .

c [mM]	$\delta \text{ H}^c$ [ppm]	$\delta \text{ H}^{c'}$ [ppm]	$\delta \text{ H}^{a'}$ [ppm]	$\delta \text{ H}^6$ [ppm]	c [mM]	$\delta \text{ H}^c$ [ppm]	$\delta \text{ H}^{c'}$ [ppm]	$\delta \text{ H}^{a'}$ [ppm]	$\delta \text{ H}^6$ [ppm]
10	9.54	9.30	8.36	8.06	10	9.89	9.49	9.05	7.88
5.0	9.65	9.47	8.62	7.99	5.0	9.92	9.57	9.14	7.87
1.0	9.82	9.75	9.07	7.74	1.0	9.91	9.69	9.27	7.78
0.50	9.89	9.86	9.23	7.65	0.50	9.91	9.79	9.38	7.74
0.25	9.92	9.90	9.29	7.62	0.25	9.91	9.91	9.49	7.68

d_3 with regard to the chemical shifts of protons $\text{H}^c, \text{H}^{c'}, \text{H}^{a'}$ and H^6 .

Emission spectroscopy

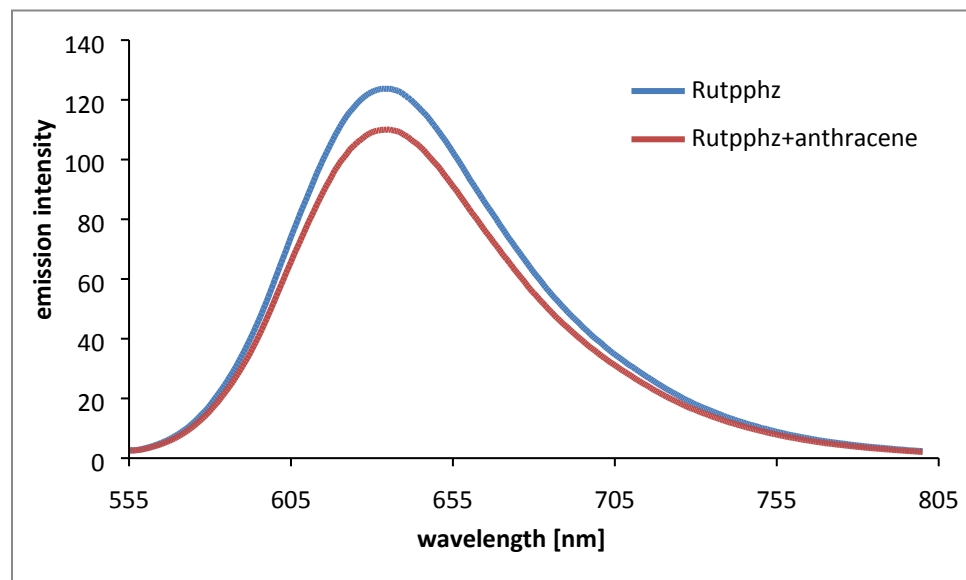


Figure S13 Emission quenching by addition of anthracene: emission of **Rutpphz** ($c = 1.0 \mu M$) in acetonitrile (blue line); addition of anthracene ($c = 80 \mu M$) leads to a decrease of emission intensity (red line). Excitation wavelength: 470 nm.

	Rutpphz	Rutpphz + anthracene
peak area	10348.65	9548.77
emission queching		7.7 %

Table S4 Emission quenching by addition of anthracene ($c = 80 \mu M$) to **Rutpphz** ($c = 1.0 \mu M$) in acetonitrile by 7.7%.

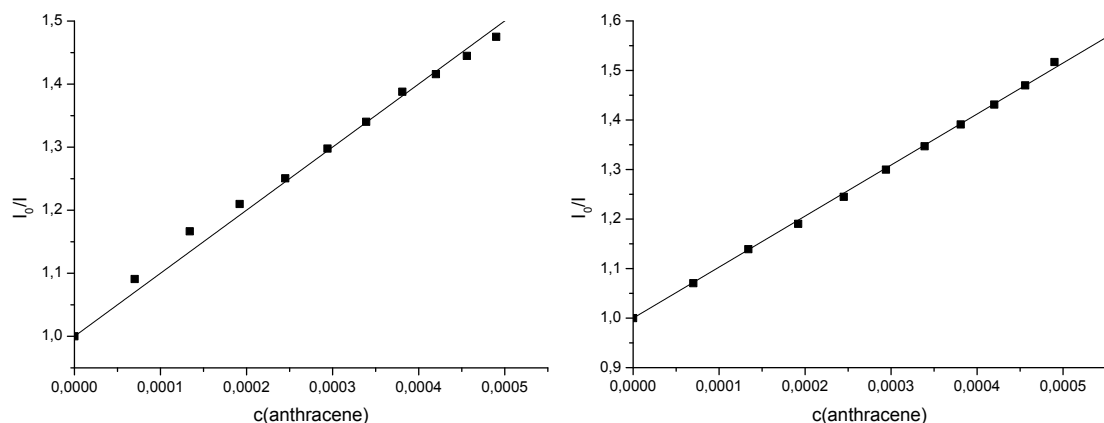


Figure S14 Stern Volmer analysis of emission quenching of **Rutpphz** ($3.5 \mu M$) by anthracene at $20^\circ C$ (left) and $35^\circ C$ (right). The linear fit gives the dynamic Stern Volmer constants $K_{SV}(20^\circ C) = 1000 \pm 14 M^{-1}$ and $K_{SV}(35^\circ C) = 1030 \pm 5 M^{-1}$. Excitation wavelength: 470 nm.

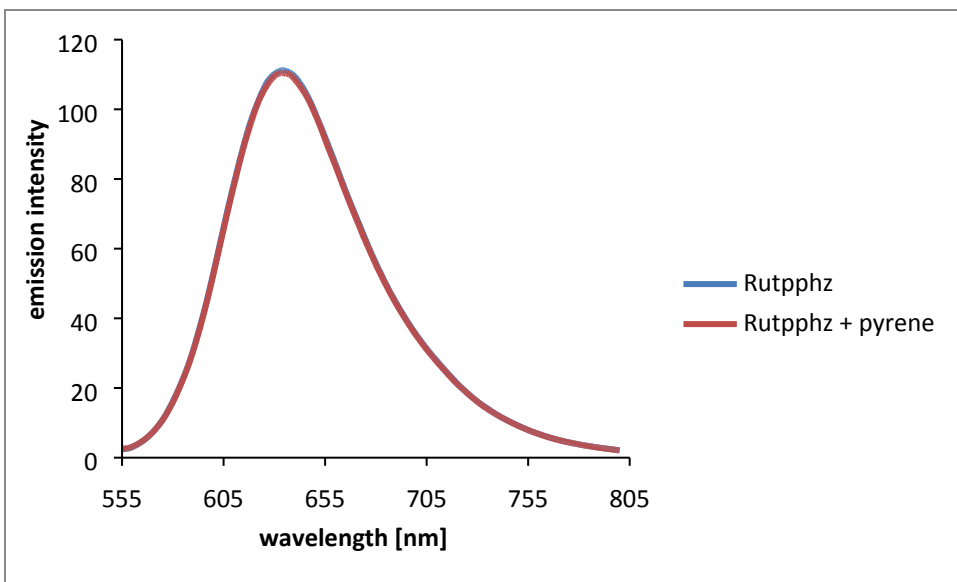


Figure S15 Emission before and after addition of pyrene: emission of **Rutpphz** ($c = 1.0 \mu M$) in acetonitrile (blue line); emission after addition of pyrene ($c = 80 \mu M$) (red line). Excitation wavelength: 470 nm.

Emission spectra of the water quenching experiment

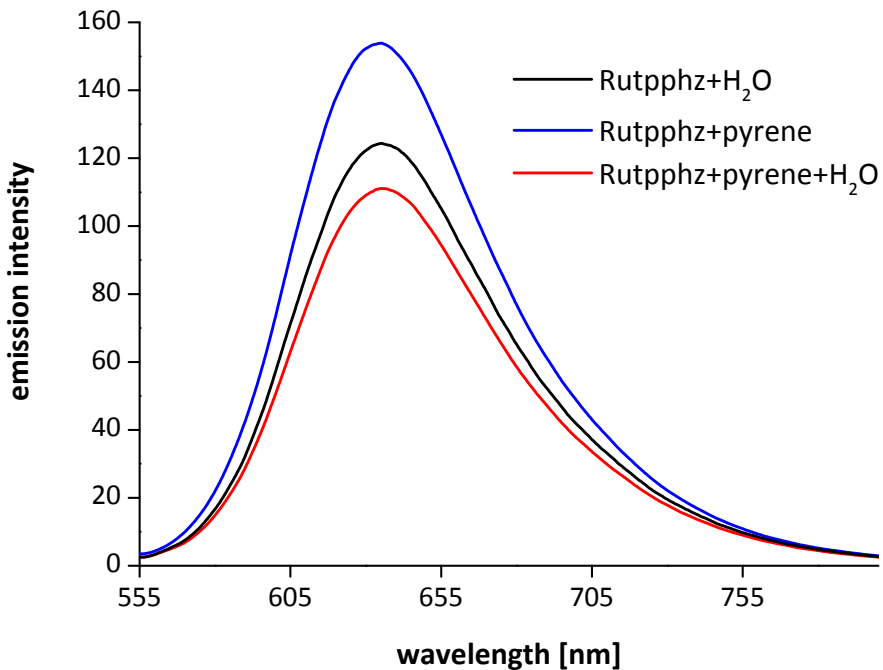


Figure S16 Analysis of the influence of pyrene on the emission quenching of **Rutpphz** by water. Excitation wavelength: 470 nm; $c(\text{Rutpphz}) = 1 \mu M$; $c(\text{pyrene}) = 80 \mu M$; $c(H_2O) = 1.8 M$.

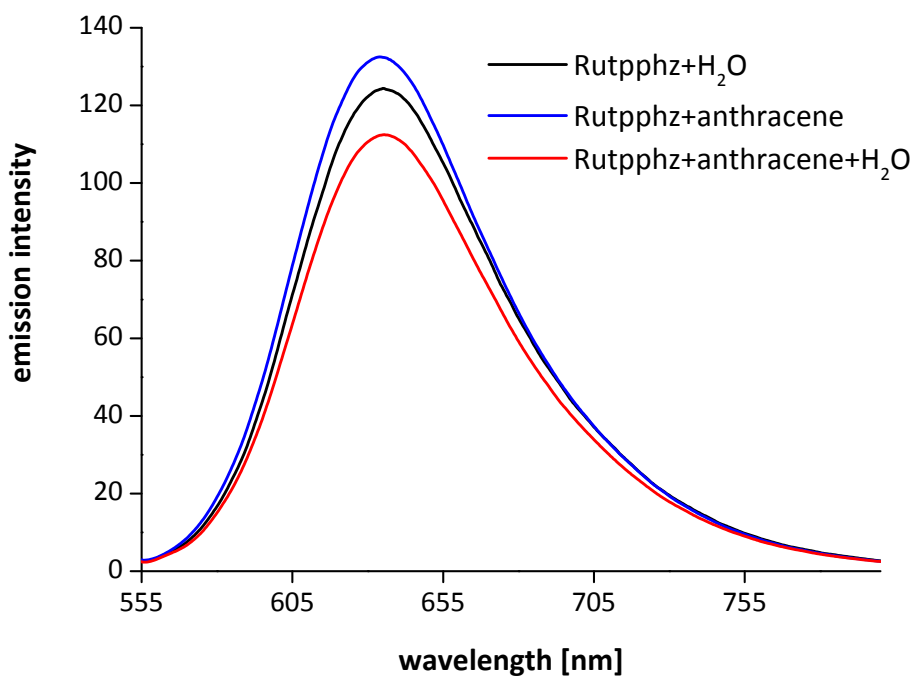


Figure S17 Analysis of the influence of anthracene on the emission quenching of **Rutpphz** by water. Excitation wavelength: 470 nm; $c(\text{Rutpphz}) = 1 \mu\text{M}$; $c(\text{anthracene}) = 80 \mu\text{M}$; $c(\text{H}_2\text{O}) = 1.8 \text{ M}$.

Mass spectrometry

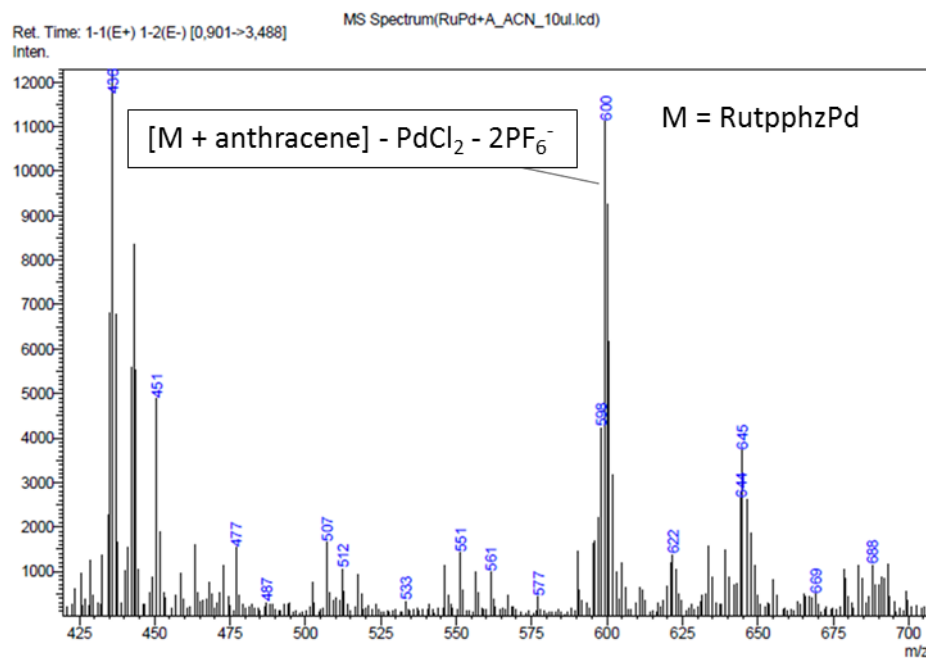


Figure S18 ESI mass spectrum of **RutpphzPd** ($c = 1.0 \mu\text{M}$) and anthracene (80-fold excess) in acetonitrile.

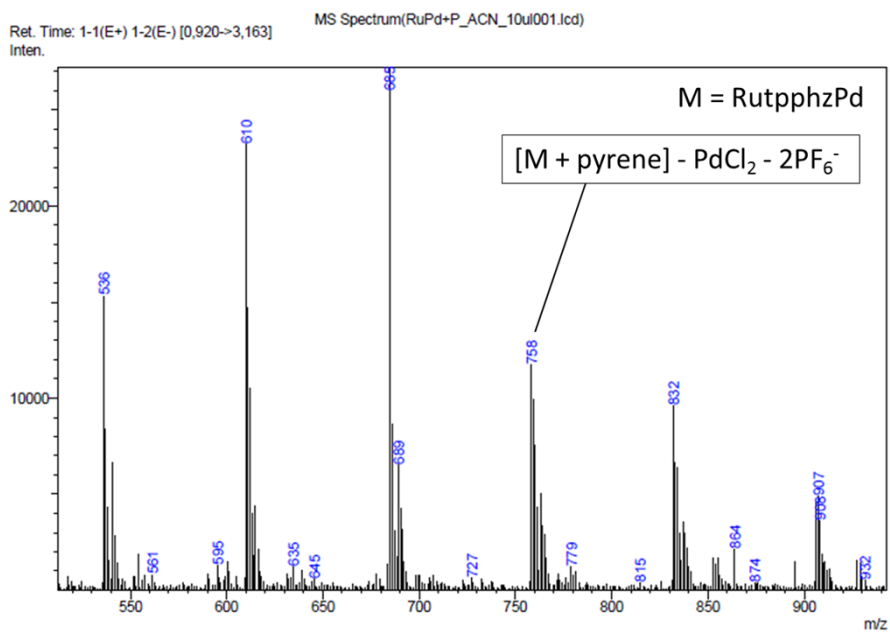


Figure S19 ESI mass spectrum of **RutpphzPd** ($c = 1.0 \mu\text{M}$) and pyrene (80-fold excess) in acetonitrile.

Table S5 Crystallographic data for $[(tbbpy)Ru(tpphz)Pd(Cl_2)][Mo_8O_{26}] \cdot ca. 18 DMF \cdot 2 H_2O$

Table 1. Crystal data and structure refinement for p-1.

Empirical formula	C168 H232 Cl4 Mo8 N38 O44 Pd2 Ru2
Formula weight	4812.16
Temperature	293(2) K
Wavelength	0.71073 Å
Crystal system	Triclinic
Space group	P -1
Unit cell dimensions	a = 14.6799(3) Å a= 103.457(2)°. b = 19.1828(4) Å b= 106.027(2)°. c = 22.7309(5) Å g = 104.881(2)°.
Volume	5619.3(2) Å ³
Z	1
Density (calculated)	1.422 Mg/m ³
Absorption coefficient	0.836 mm ⁻¹
F(000)	2442
Crystal size	0.1336 x 0.067 x 0.0623 mm ³
Theta range for data collection	3.400 to 26.372°.
Index ranges	-18<=h<=18, -23<=k<=23, -28<=l<=28
Reflections collected	72507
Independent reflections	22937 [R(int) = 0.0432]
Completeness to theta = 25.242°	99.7 %
Refinement method	Full-matrix least-squares on F ²
Data / restraints / parameters	22937 / 20 / 1007
Goodness-of-fit on F ²	0.956
Final R indices [I>2sigma(I)]	R1 = 0.0447, wR2 = 0.1212
R indices (all data)	R1 = 0.0748, wR2 = 0.1266
Largest diff. peak and hole	0.939 and -0.534 e·Å ⁻³

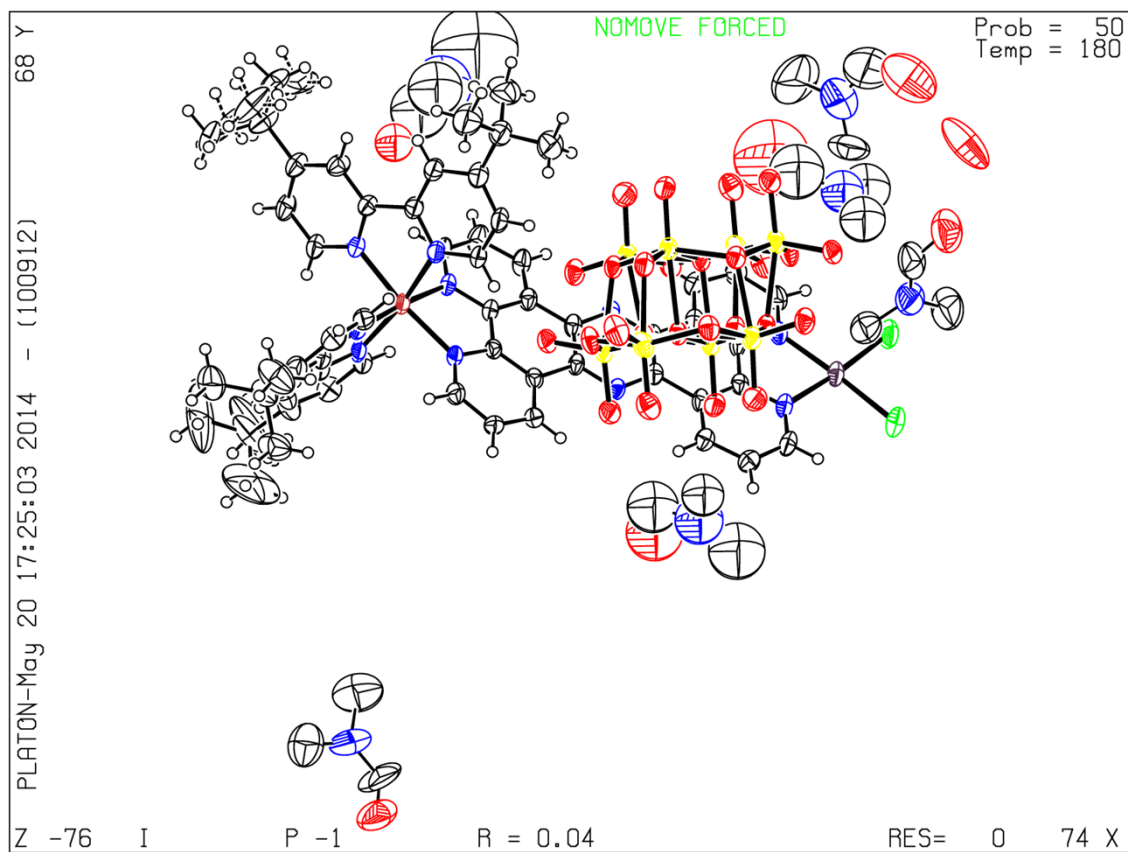


Figure S20 ORTEP representation of $[(\text{tbbpy})_2\text{Ru}(\text{tpphz})\text{Pd}(\text{Cl})_2]_2(\text{Mo}_8\text{O}_{26})$ (CCDC 987314), thermal ellipsoids given at 50 % probability.

Disorder of the solvent DMF molecules:

During the structure refinement, disorder of several DMF solvent molecules within the crystal lattice was observed. The DMF molecules were assigned and refined isotropically or anisotropically. For several DMF molecules, the positional parameters were fixed to give a stable refinement. As not all solvent positions could be assigned to give a stable refinement, the Platon SQUEEZE routine was employed to account for diffuse electron density within the lattice. The SQUEEZE routine gave a void volume of 1443 \AA^3 (ca. 23 % of the unit cell) with a integral electron density of 213 e^- . The “solvent-accessible void” routine within the CCDC Mercury program suite (v.3.3) gave a solvent-accessible void space of 614 \AA^3 , this volume is estimated to contain 8 DMF molecules (molecular volume for DMF ca 90 \AA^3). In order to further illustrate this algorithm we show the “voids” in figure S21.

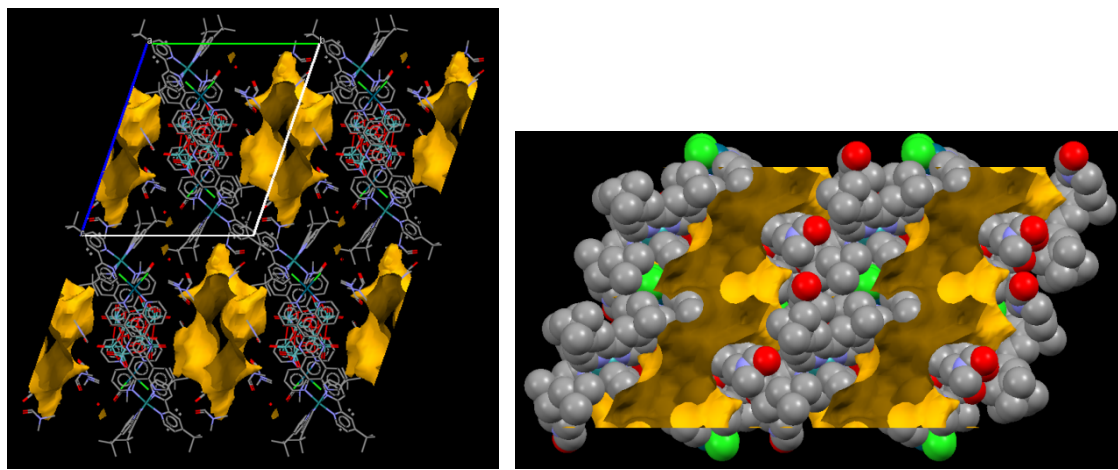


Fig S21: View of the solvent accessible voids in compound $[(tbbpy)_2Ru(tpphz)Pd(Cl)_2]_2(Mo_8O_{26})$ (CCDC 987314) along the crystallographic *a*-axis (left) and along the crystallographic *b*-axis (right).

¹ L. Fielding, *Tetrahedron* 2006, **56**, 6151.

² P. Thordarson, *Chem. Soc. Rev.* 2011, **40**, 1305.

³ a) V. Steullet and D. W. Dixon, *Chem. Soc., Perkin Trans. 2*, 1999, 1547; b) N. R. de Tacconi, R. Chitakunye, F. M. MacDonnell and R. O. Lezna, *J. Phys. Chem. A*, 2008, **112**, 497.